water

Text S1: An example for estimation of climate response to INDC

Emissions

We use the INDC emissions data submitted by 192 countries according to the Paris Agreement. The INDC dataset is continuously updated and can be obtained from the UNFCCC website (UNFCCC, 2018). The reported emission targets of countries vary from absolute emission targets to those relative to a base year level, or emission reduction targets relative to a baseline emission scenario. We analyzed and extracted most countries' emission targets. In the 165 INDCs, 124 were assessed and quantified (covering 151 countries), which together account for 93.6% of global GHG emissions. For other INDCs, the mitigation targets cannot be assessed due to lack of quantified goals, and they together account for only a small part of global GHG emissions. For more details of the global INDC emission calculations refer to [1]. Global INDC emissions before 2030 were estimated by summing up national INDC emissions.

Simulations of future emissions from 28 socioeconomic models were used to extend the INDC scenarios until the end of this century. We considered the rate of decarbonization, carbon capture and storage technology (CCS), energy structure improvement, and time to carbon neutralization, etc. Here, we take into account many possible interpretations of "INDC mitigation actions" as available in the scenarios that contributed to the IPCC AR5 Scenario Database. We use scenarios that conform to 2030 GHG emission levels consistent with the INDCs (50-56 $GtCO_2eq/yr$) and assume no sudden changes in climate action over the 21st century. Considering the difficulty and uncertainty of carbon removal technology in the future, we take a conservative approach regarding the future availability of negative emissions technologies and scenarios with CCS > 15 Gt CO_2eq/yr are eliminated.

We further classify these emission pathways into six groups based on some key characteristics (e.g. emission targets for specific years, renewable energy structure, and the amount of CCS), shown in Figure S1. Group I (baseline scenario) contains scenarios without any additional climate policies nor mitigation actions, where the GHG emissions continue to grow according to current trends. Group II is similar to the baseline scenario but allows for lower energy intensity in the future. Group III represents a weak-policy baseline scenario considering existing climate policies, a weak interpretation (e.g., 2020 Copenhagen Pledges), and extrapolation of these targets beyond 2020 based on emissions intensity. Global emissions were assumed to peak in 2030 in Groups IV to VI. Specifically, Group IV can be described as a "continued action" pathway. The relatively constant decarbonization rates were roughly followed for the period after 2030. The overall trend of Group V is close to Group IV, but more rapid mitigation after 2030 is the distinguishing characteristic. Group VI involves CCS action accelerating decarbonization and determining negative emissions in some pathways.

To assess the global mean warming level induced by INDC emission scenarios, we use the 78 climate sensitivity experiments from the earth system models (ESMs) ensemble of CMIP5 [2] and estimate the possible corresponding global mean temperature rise for various emission scenarios [1,3]. we also integrated several other studies (temperature rise levels for some pathways have been provided) [4-7]. For example, the United Nations Environment Program (UNEP) issued the "Emissions Gap Report" [7] and hypothesized that global emissions in accordance with the INDC development would result in a global warming of 3°C–4°C (probability >66%) by 2100. Rogelj et al. (2016)[5] showed that under the INDC continuous mitigation pathways, the median temperature rise at the end of this century will be estimated to be ~2.6°C–3.1°C and the temperature increase will likely be stronger. Based on simulations of the CMIP5 Earth System Models ensemble, Wang et al. (2018)[1] pointed out that the INDC emissions would lead to a mean global warming of 1.4°C (1.3°C–1.7°C) in 2030 and 3.2°C (2.6°C–4.3°C) in 2100. After a comprehensive assessment, we determined the most likely ranges of temperature increases for each emission pathway of INDCs, as shown in Figure S1.

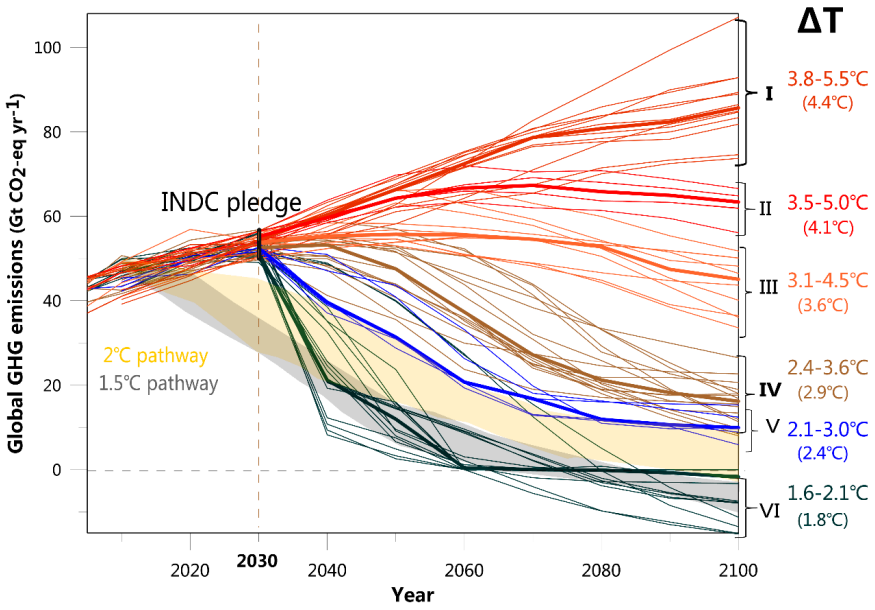

Figure 1. Future emission pathways analyzed in this example. The black vertical line represents the range of conditional and unconditional INDC pledges in 2030; thin lines in different colors show the selected emission pathways clustered into the six groups. The range of the 1.5 °C and 2 °C pathways are plotted for reference, in grey and orange shaded areas, respectively [4,8,9]. The estimates of current warming above the pre-industrial level (ΔT) for each scenario group are labelled on the right (uncertainty range of 33-66% and median in brackets).

Table S2. Global climate models used in this study.

Table S1. Details of the 14 CMIP5 global climate models used in this research.

Model	Institute	Country	Horizontal Resolution
BCC-CSM1-1	Beijing Climate Center	China	128×64
CanESM2	Canadian Centre for Climate Modelling and Analysis	Canada	128×64
CESM1-BGC	National Center for Atmospheric Research	USA	288×192
CMCC-CM	Centro Euro-Mediterraneo sui Cambiamenti Climatici	Italy	480×240
CSIRO-Mk3-6-0	Commonwealth Scientific and Industrial Research Organization/ Queensland Climate Change Centre of Excellence	Australia	192×96
EC-EARTH	EC-EARTH consortium		320×160
FGOALS-g2	Institute of Atmospheric Physics, Chinese Academy of Sciences	China	128×60
FGOALS-s2	Institute of Atmospheric Physics, Chinese Academy of Sciences	China	128×108
GFDL-ESM2G	Geophysical Fluid Dynamics Laboratory	USA	144×90
HadGEM2-CC	Met Office Hadley Centre	UK	192×145
HadGEM2-ES	Met Office Hadley Centre	UK	192×145
IPSL-CM5B-LR	Institut Pierre Simon Laplace	France	96×96
MIROC5	Atmosphere and Ocean Research Institute (The University of Tokyo), National Institute for Environmental Studies, and Japan Agency for Marine-Earth Science and Technology	Japan	256×128
MRI-CGCM3	Meteorological Research Institute	Japan	320×160

Text S3: The time-slice approach

This study is based on the historical run of the past approximately 150 years with all forcings, and the 21st century projection forced by the RCP8.5 scenario within the CMIP5 framework [2]. The time series of globally averaged surface air temperature is smoothed by a 21-year running mean to filter out the inter-annual variability under the historical run and RCP scenarios for individual models, the 21-year time-slice used for this average include the median year for which global mean surface temperature crosses a given warming target (ΔT_{INDC}, or 1.5°C, 2.0°C), as well as the 10 years preceding and following the median year. For time series of other climate indicators, the method above can be applied for individual models, relate various indicators to global mean warming.

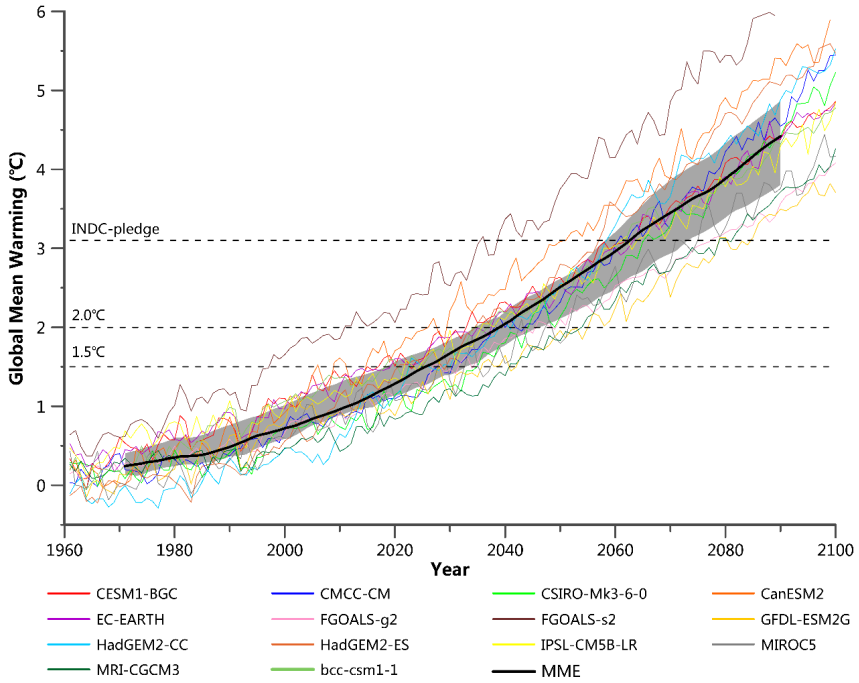

Figure S2. series of global mean annual temperature changes relative to the baseline climatology of the pre-industrial (1861–1900), as derived from individual GCMs under RCP8.5 (thin line in different colors). Multi-model ensemble with 21-year running mean (black bold line and shade) is also shown on the graph. The horizontal dashed lines indicate a given warming target.

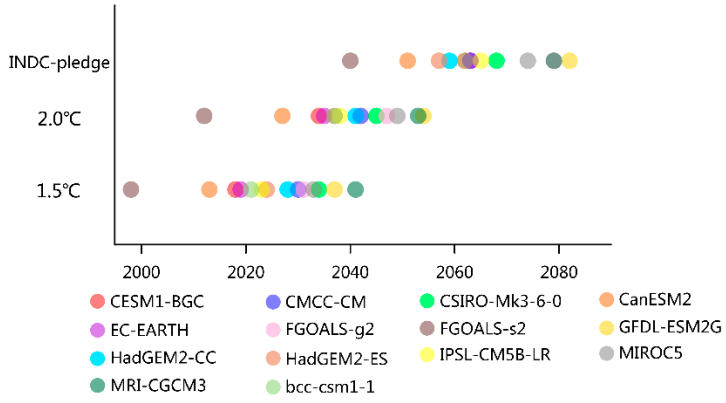

Figure S3. Median years projected by the 14 CMIP5 models for three global warming targets (ΔT_{INDC}, 1.5°C, and 2.0°C) under the RCP8.5 scenario.

Text S4: Sub-regions in China

Table S2. Details of eight sub-regions in China [10].

Sub-region name	Latitude	Longitude
Northeast China (**NEC**)	39°~54°N	119°~134°E
North China (**NC**)	36°~46°N	111°~119°E
East China (**EC**)	27°~36°N	116°~122°E
Central China (**CC**)	27°~36°N	106°~116°E
South China (**SC**)	20°~27°N	106°~120°E
Tibetan Plateau (**SEC1**)	27°~36°N	77°~106°E
Southwest China (**SEC2**)	22°~27°N	98°~106°E
Northwest China (**NWC**)	36°~46°N	75°~111°E

Text S5: Evaluation of precipitation extremes in China simulated by CMIP5 models

Compared to temperature extremes, precipitation extremes are more complex climate events. It is much more difficult for climate models to simulate the features of precipitation extremes [11]. As shown in Figure S4, the observed linear trends for Rx5day, R25, and SDII in China from 1961 to 2005 are 0.166 mm/10a, 0.062 days/10a, and 0.059 (mm·day^{-1})/10a, respectively, which indicates that heavy precipitation extremes have slightly increased across China as a whole. However, the linear trends in these three indices as simulated by the model ensemble are 1.07 mm/10a, 0.032 days/10a, and 0.034 (mm·day^{-1})/10a, respectively. Although the MME generally captures the positive trends in extreme heavy precipitation events, the values of the simulated trends are different from those of the observed trends.

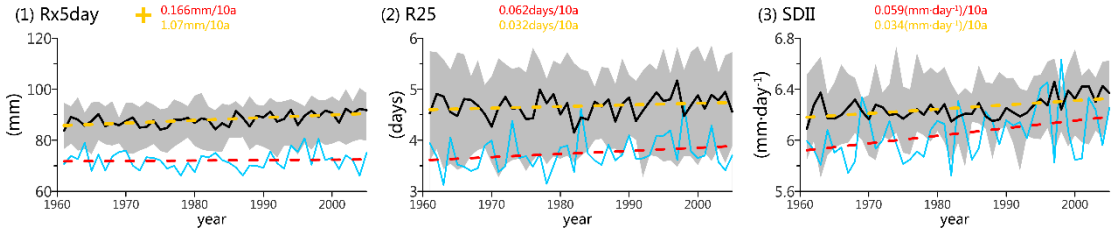

Figure S4. Observed (blue line) and simulated (black line and shade, multi-model median and interquartile range, respectively) time series of three extreme precipitation indices from 1961 to 2005. linear trends of observation (dotted line in red) and multi-model median (dotted line in yellow) are shown in same graph. Yellow cross denotes the linear trend passed the 95% confidence level.

The multi-model ensemble slightly overestimates the intensity and frequency of extreme precipitation across China, but can well reproduce the spatial pattern of extreme precipitation events (Figure S5). The relative bias for Rx5day, R25, and SDII between the MME and the observation data is 25.7, 27.0, and 3.3 %, respectively. The spatial standard deviation of the observation data (σ_{obs}) is close to that of multi-model ensemble (σ_{MME}), ratios ($\sigma_{MME}/\sigma_{obs}$) for Rx5day, R25, and SDII between the MME and the observation data is 25.7, 27.0, and 3.3 %, respectively. are 1.01, 0.93, and 0.91, respectively. In terms of the spatial distribution of precipitation extremes, the spatial correlation coefficients between MME and the observed data for the three extreme precipitation indices range are 0.85, 0.82, and 0.88, respectively.

The three extreme precipitation indices display similar spatial distribution patterns related to bias (Figure S5). There is a significant wet bias in most regions, especially for the south eastern periphery of the Tibetan Plateau. While there is a large dry bias in the middle and lower reaches of the Yangtze River and Southeast China, which is consistent with the results provided by [12]. It is noteworthy that a strong positive precipitation bias occurs along the southeastern periphery of Tibetan Plateau, a finding that is consistent with a number of previous results [12,13].

The analysis above indicates that the MME of 14 CMIP5 models can accurately reproduce the spatial features of observed precipitation extremes in China, although they are limited in their ability to capture temporal features.

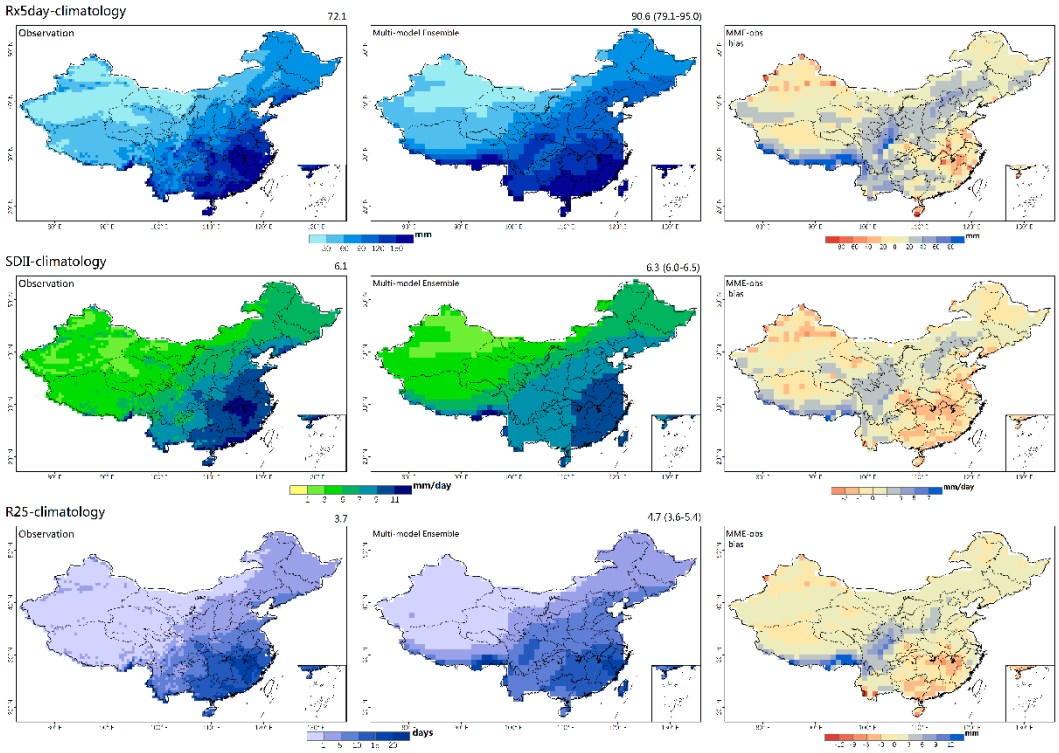

Figure S5. Spatial distribution of extreme precipitation indices for Rx5day (unit: days), SDII (unit: mm·day^{-1}), and R25 (unit: days) during the period of present (1985–2005). Column 1: observation; Column 2: MME; Column 3: bias (model ensemble simulation minus observation).

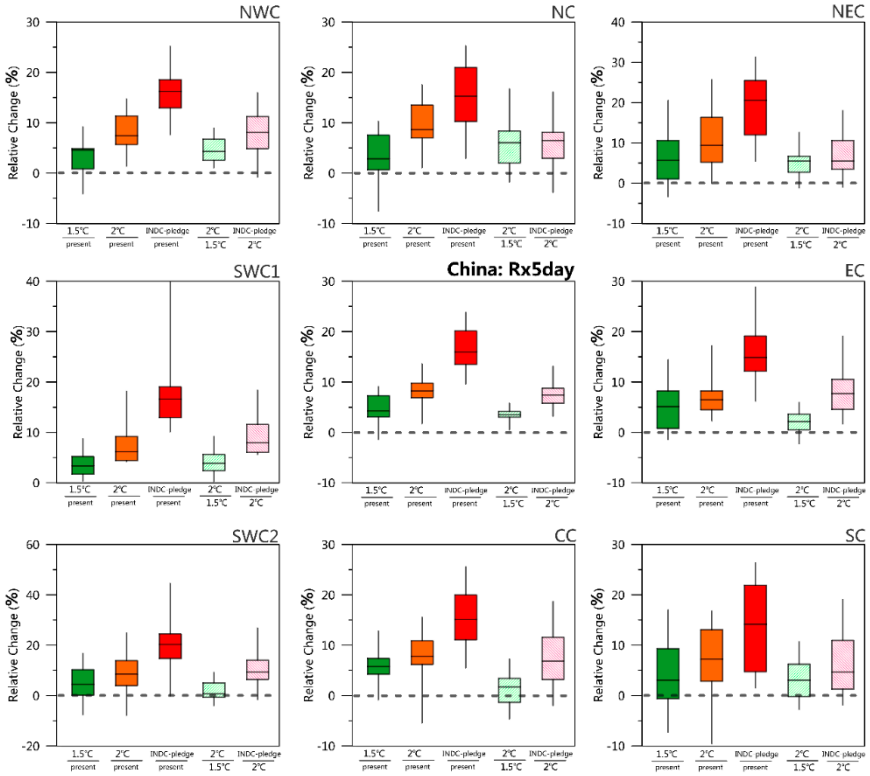

Figure S6. Regional average differences among different scenarios in the annual Rx5day in China and its eight sub-regions, based on the multi-model mean ensemble. Boxes (Whiskers) indicate the 25th and 75th percentiles (maximum and minimum) of 14 climate models, and the horizontal lines represent the multi-model median. Scenarios are the same as Figure 5, with corresponding colors. The differences between different sets of scenarios are labelled on the x-axis. The first three bars show differences for each scenario (1.5 °C, 2.0 °C, and INDC-pledge) relative to the present-day baseline scenario, and the last two bars show differences between the 1.5 °C and 2.0 °C scenarios, and INDC scenario relative to the 2.0 °C scenario, as labelled. Eight sub-regions (labelled in top left corner) are defined in Text S4.

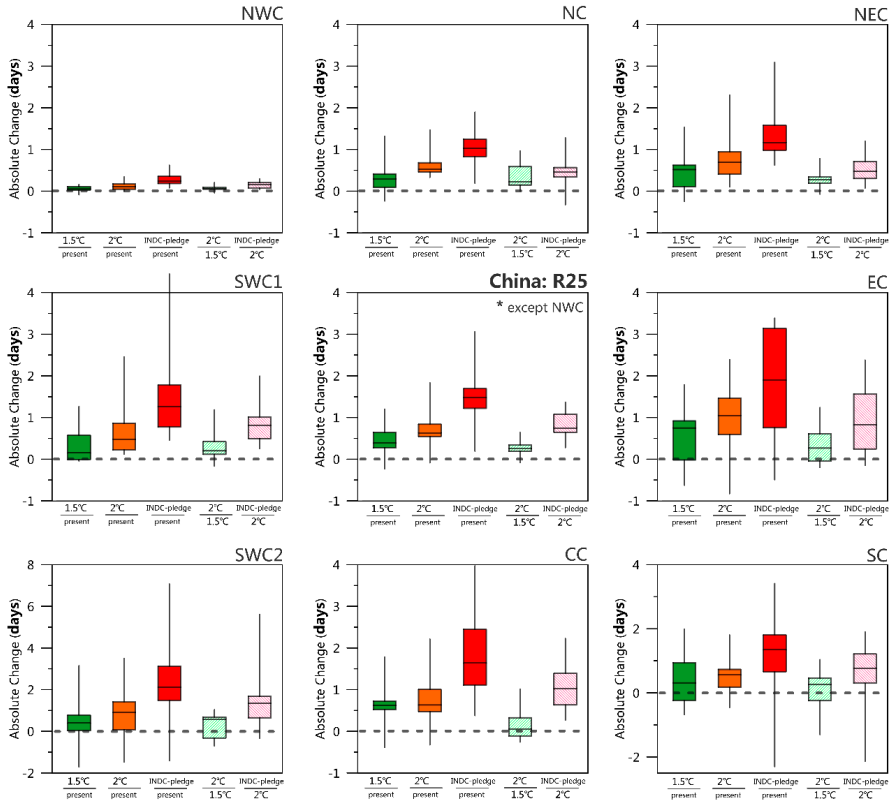

Figure S7. Corresponds to Figure S6, but for R25. *The nationally average of R25 (the central sub-figure), does not include NWC.

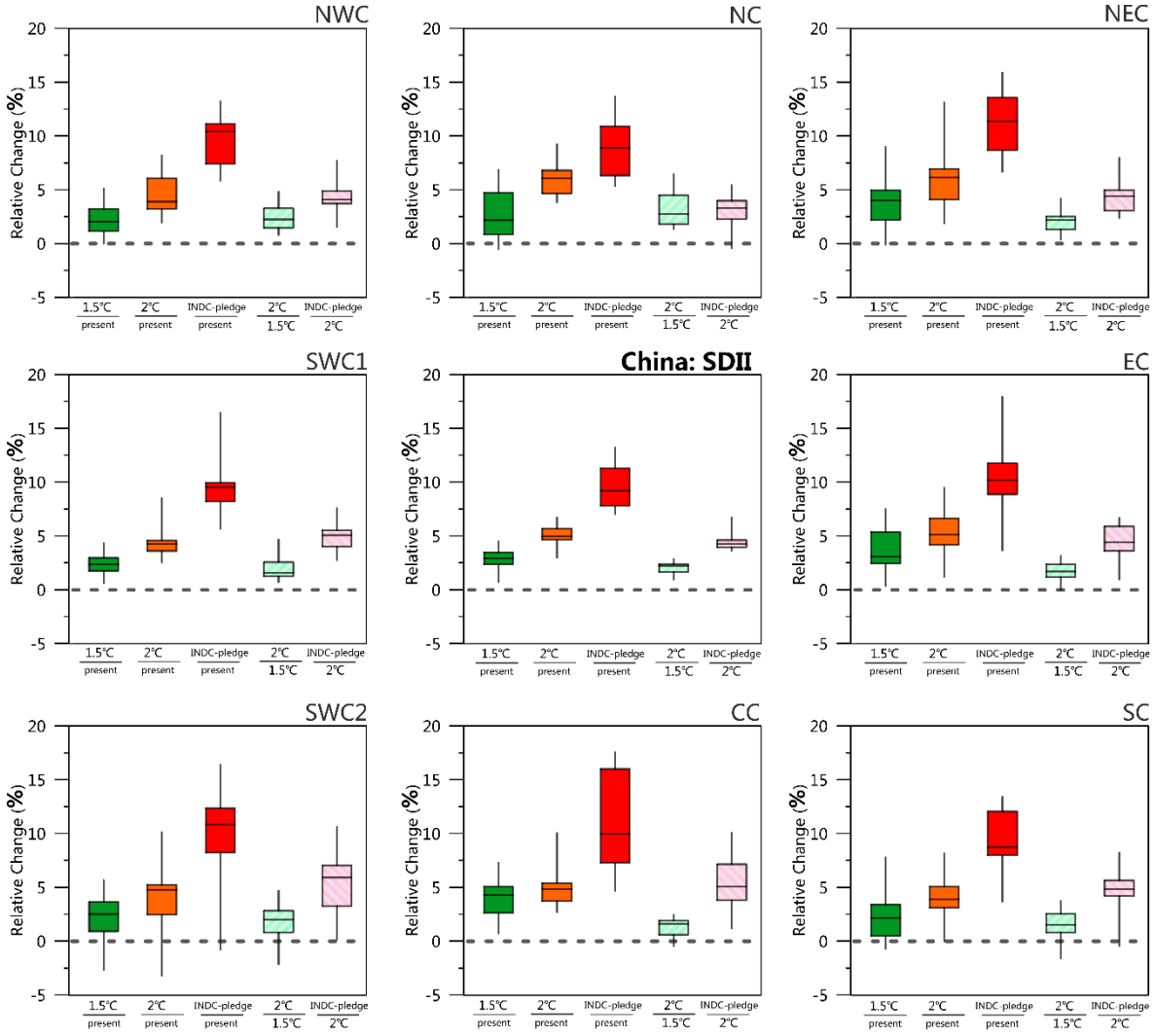

Figure S8. Corresponds to Figure S6, but for SDII.

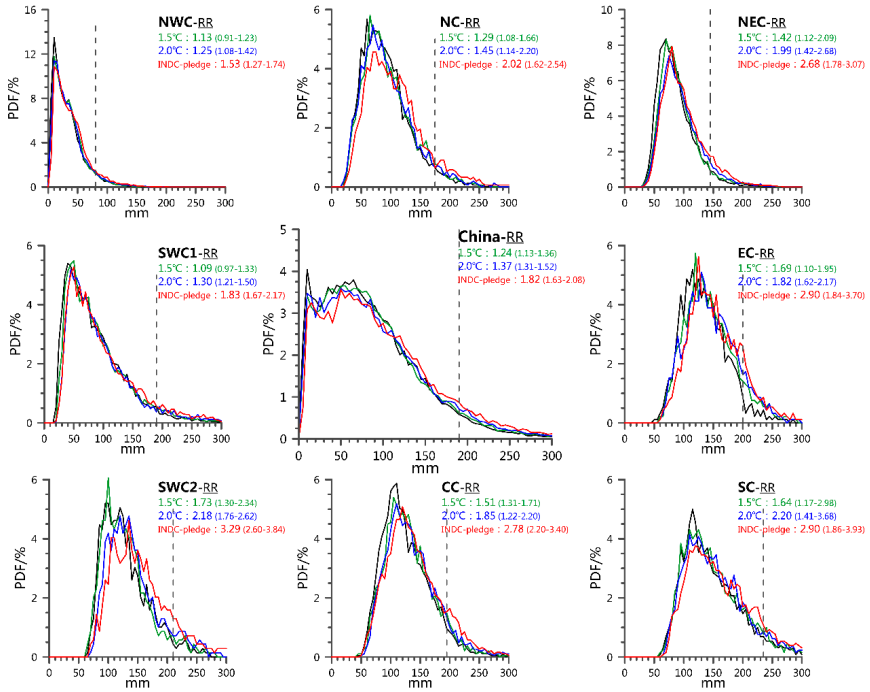

Figure S9. Frequency distributions of extreme precipitation indices Rx5day over China and its eight sub-regions. Black lines indicate the results during 1985-2005. Green, blue, and red lines indicate the results during 1.5°C, 2.0°C, and ΔT_{INDC} warming period, respectively. The dashed lines indicate the 5% extreme values for baseline period 1985-2005. Risk ratios (RRs) for three scenarios labeled on the top-right (including medians and interquartile ranges).

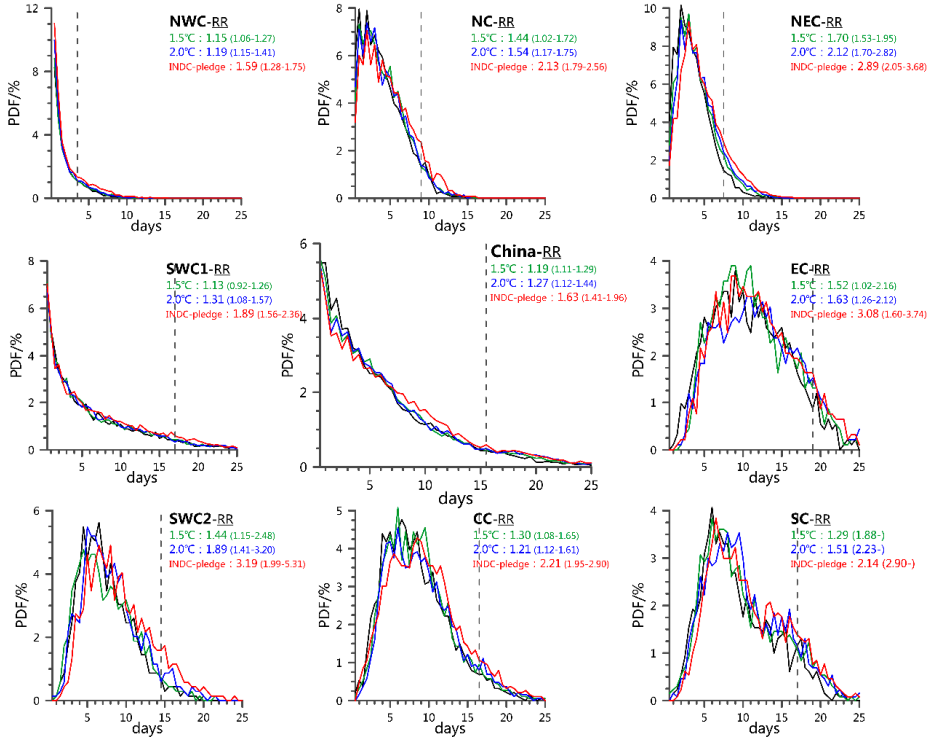

Figure S10. Corresponds to Figure S9, but for R25. Zero values of R25 are omitted.

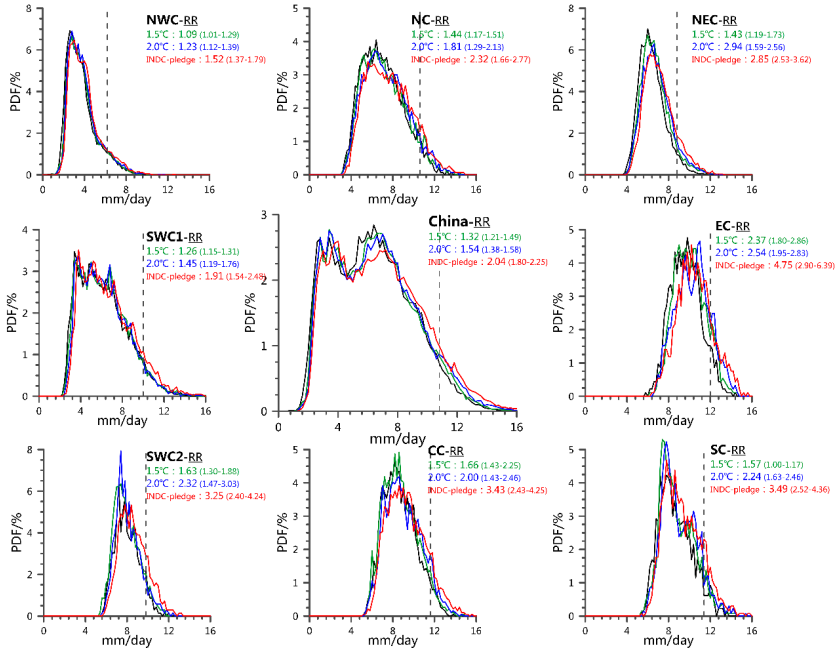

Figure S11. Corresponds to Figure S9, but for SDII.

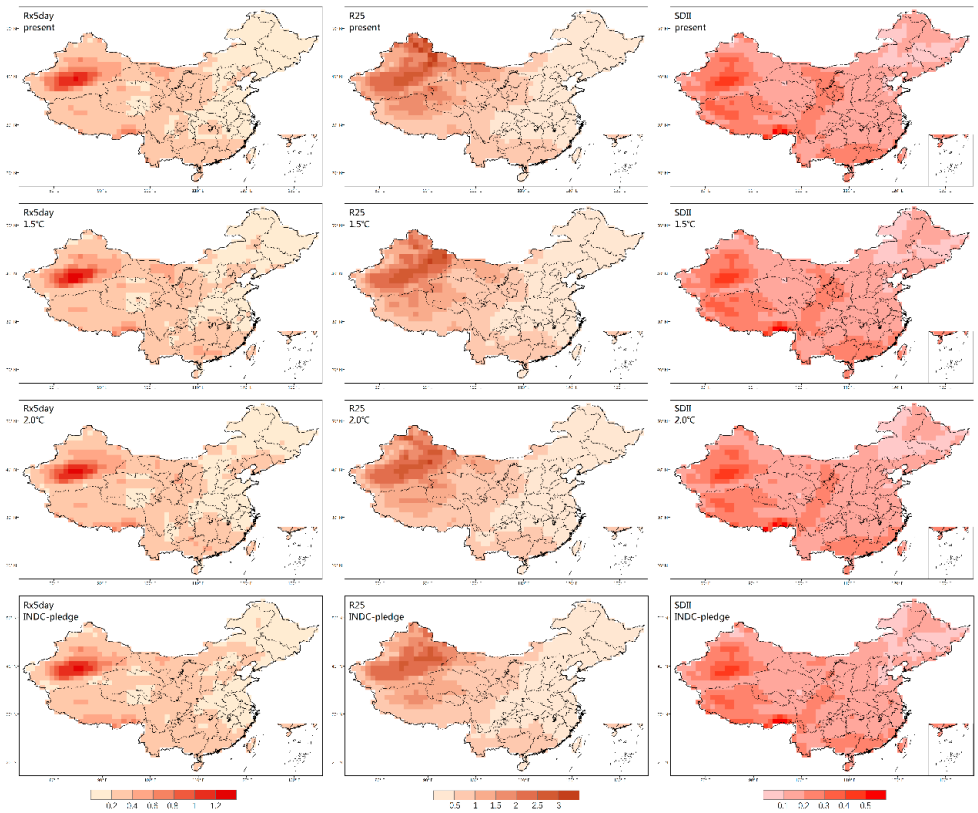

Figure S12. Spatial distribution of the intermodel coefficient of variations (C_v) of three extreme precipitation indices simulated by the 14 CMIP5 models for scenarios of present, 1.5°C, 2.0°C, and INDC-pledge.

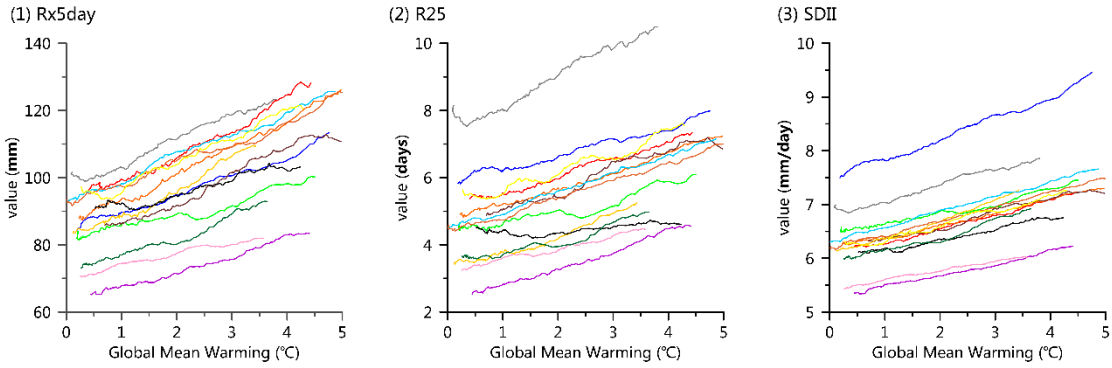

Figure S13. Three extreme precipitation indices over China (regional average) simulated by 14 individual CMIP5 models (in different color lines), with corresponding global mean warming.

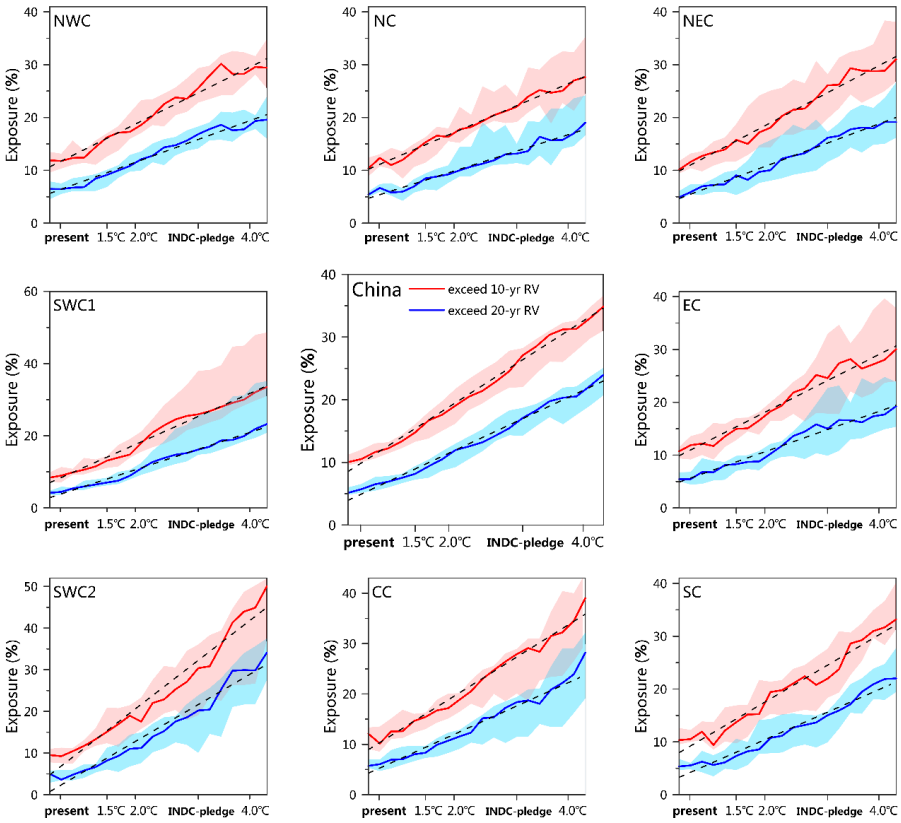

Figure S14. Multi-model ensemble areal exposure to heavy rainfall of different return values (RVs). Corresponds to Figure 7, but for areal exposure. Corresponds to this figure, calculation results of individual models refer to Figure S17 and S18.

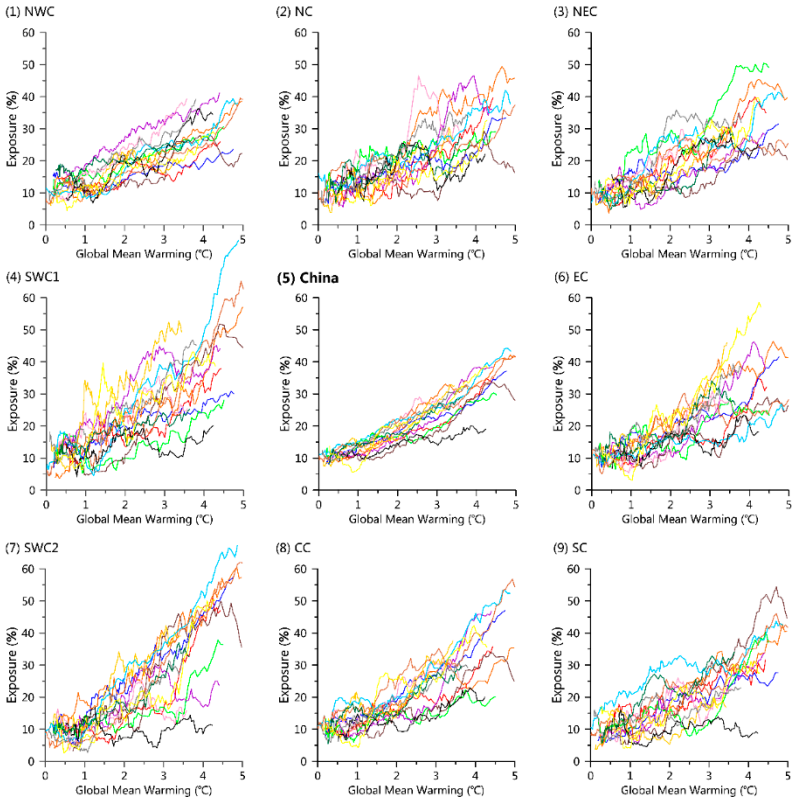

Figure S15. Population exposure to heavy precipitation events of 10-year RV, at corresponding warming levels, over Asia and eight sub-regions (labelled in top left corner), based on results of individual models (line in different colors).

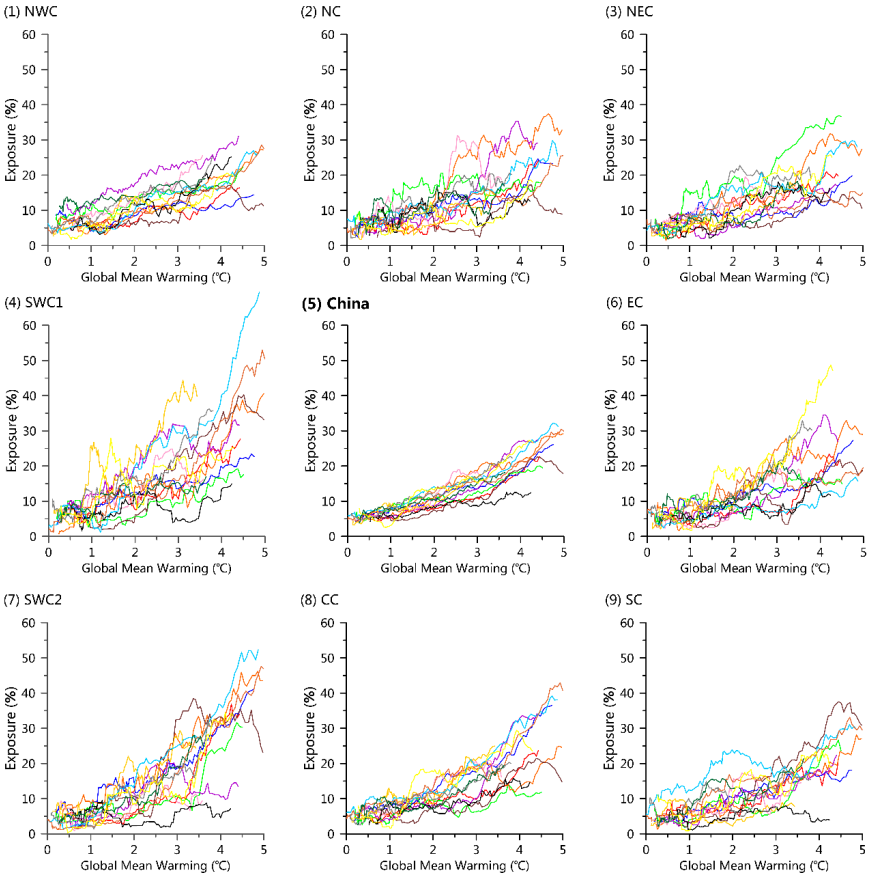

Figure S16. Corresponds to Figure S15, but for population exposure to heavy precipitation events of 20-year RV.

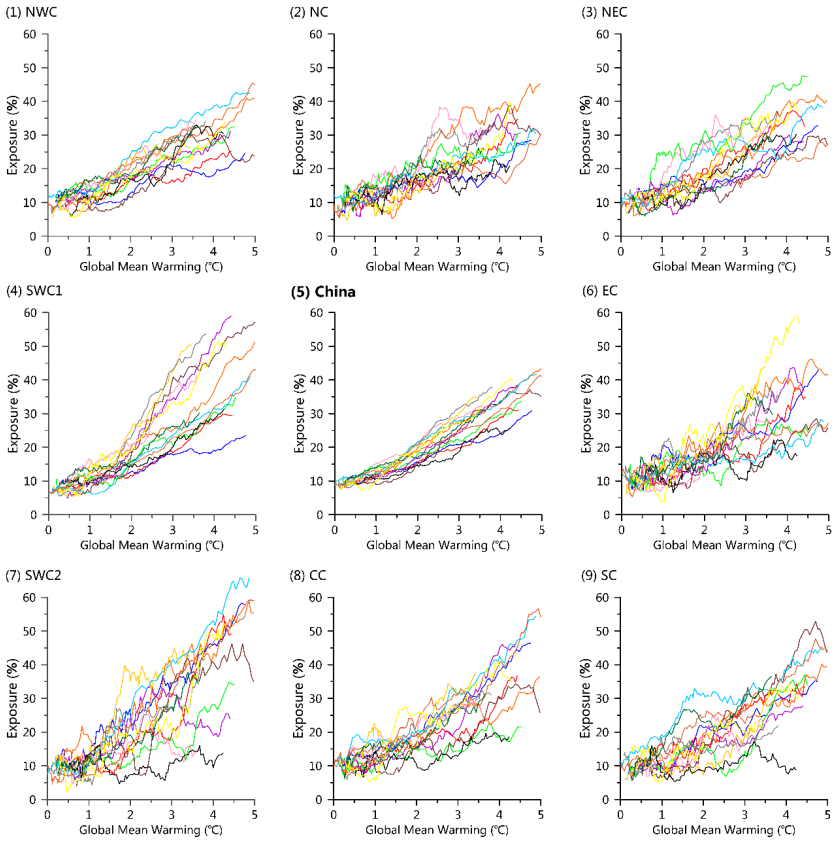

Figure S17. Areal exposure to heavy precipitation events of 10-yr RV, at corresponding warming levels, over Asia and eight sub-regions (labelled in top left corner), based on results of individual models (line in different colors).

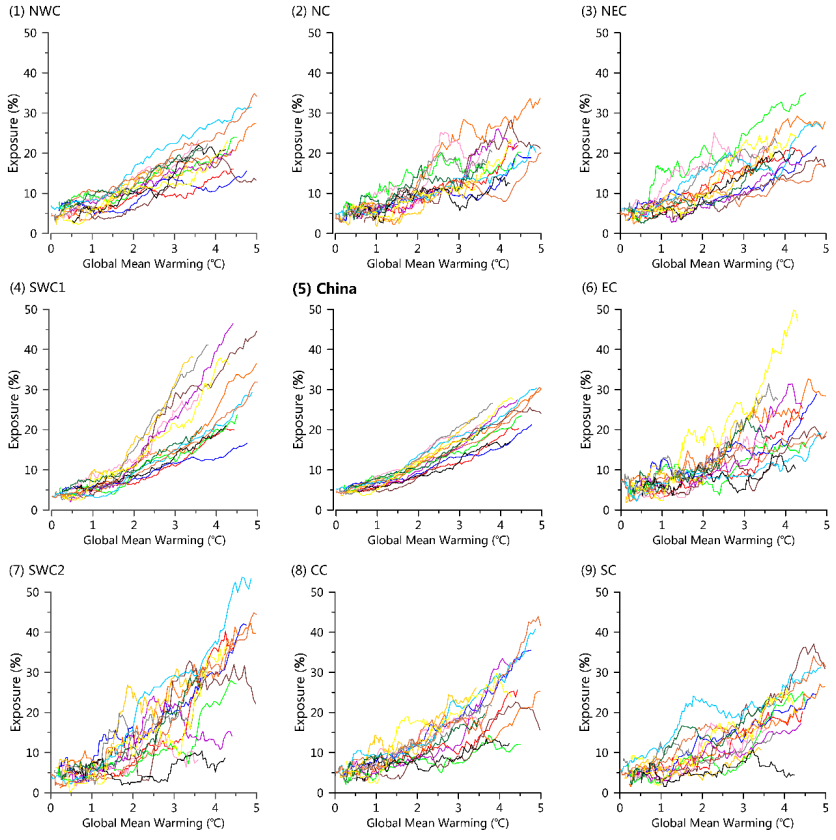

Figure S18. Corresponds to Figure S17, but for population precipitation events of 20-yr RV.

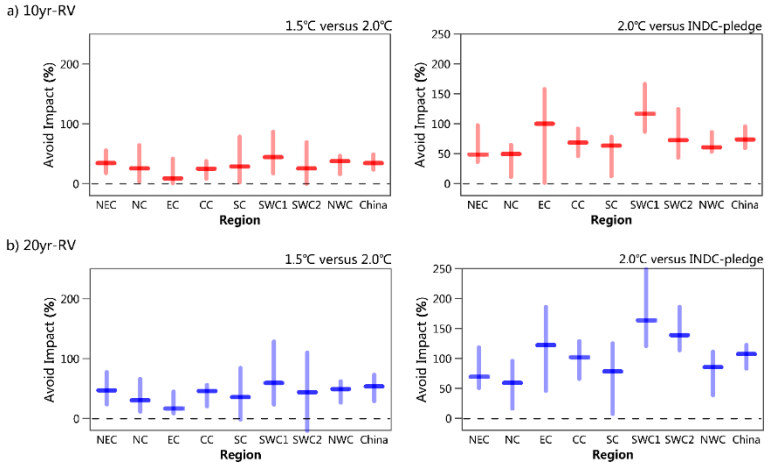

Figure S19. Corresponds to Figure 8, but for areal exposure.

References

1. Wang, F.; Tokarska, K.B.; Zhang, J.; Ge, Q.; Hao, Z.; Zhang, X.; Wu, M. Climate Warming in Response to Emission Reductions Consistent with the Paris Agreement. *Advances in Meteorology* **2018**, *2018*, 1-9, doi:10.1155/2018/2487962.
2. Taylor, K.E.; Stouffer, R.J.; Meehl, G.A. An Overview of CMIP5 and the Experiment Design. *Bulletin of the American Meteorological Society* **2011**, *93*, 485-498, doi:10.1175/BAMS-D-11-00094.1.
3. Wang, F.; Ge, Q.; Chen, D.; Luterbacher, J.; Tokarska, K.B.; Hao, Z. Global and regional climate responses to national-committed emission reductions under the Paris agreement. *Geografiska Annaler: Series A, Physical Geography* **2018**, *100*, 240-253, doi:10.1080/04353676.2018.1488538.
4. CAT. Addressing global warming. Availabe online: https://climateactiontracker.org/global/temperatures/.
5. Rogelj, J.; den Elzen, M.; Höhne, N.; Fransen, T.; Fekete, H.; Winkler, H.; Schaeffer, R.; Sha, F.; Riahi, K.; Meinshausen, M. Paris Agreement climate proposals need a boost to keep warming well below 2 °C. *Nature* **2016**, *534*, 631, doi:10.1038/nature18307
6. Sanderson, B.M.; O'Neill, B.C.; Tebaldi, C. What would it take to achieve the Paris temperature targets? *Geophysical Research Letters* **2016**, *43*, 7133-7142, doi:10.1002/2016GL069563.
7. UNEP. *The Emissions Gap Report*; Nairobi, 2017.
8. IPCC. *Climate Change 2014: Synthesis Report. Contribution of Working Groups I, II and III to the Fifth Assessment Report of the Intergovernmental Panel on Climate Change*; Cambridge University Press: Cambridge, UK, and New York, NY, USA, 2014.
9. IPCC. *Global Warming of 1.5 ºC*; Cambridge University Press: Cambridge, UK, and New York, NY, USA, 2018.
10. National Report Committee. *China's National Assessment Report on Climate Change* (in Chinese); Beijing, 2007; p 422.
11. Jiang, D.; Sui, Y.; Lang, X. Timing and associated climate change of a 2 °C global warming. *International Journal of Climatology* **2016**, *36*, 4512-4522, doi:10.1002/joc.4647.
12. Jiang, Z.; Wei, L.; Xu, J.; Li, L. *Extreme Precipitation Indices over China in CMIP5 Models. Part I: Model Evaluation*; 2015; Vol. 28, pp. 150902151739009.
13. Gao, X.; Shi, Y.; Song, R.; Giorgi, F.; Wang, Y.; Zhang, D. Reduction of future monsoon precipitation over China: comparison between a high resolution RCM simulation and the driving GCM. *Meteorology and Atmospheric Physics* **2008**, *100*, 73-86, doi:10.1007/s00703-008-0296-5.